Published in final edited form as:

Cell. 2015 June 18; 161(7): 1527–1538. doi:10.1016/j.cell.2015.05.025.

ER Stress Sensor XBP1 Controls Anti-tumor Immunity by Disrupting Dendritic Cell Homeostasis

Juan R. Cubillos-Ruiz[1,2], **Pedro C. Silberman**[1], **Melanie R. Rutkowski**[3], **Sahil Chopra**[1], **Alfredo Perales-Puchalt**[3], **Minkyung Song**[1], **Sheng Zhang**[4], **Sarah E. Bettigole**[1,2,5], **Divya Gupta**[6], **Kevin Holcomb**[6], **Lora H. Ellenson**[7], **Thomas Caputo**[6], **Ann-Hwee Lee**[7], **Jose R. Conejo-Garcia**[3], and **Laurie H. Glimcher**[1,2,*]

[1]Department of Medicine, Weill Cornell Medical College, New York, NY 10065, USA

[2]Sandra and Edward Meyer Cancer Center, Weill Cornell Medical College, New York, NY 10065, USA

[3]Tumor Microenvironment and Metastasis Program, The Wistar Institute, Philadelphia, PA 19104, USA

[4]Institute of Biotechnology, Cornell University, Ithaca, NY 14853, USA

[5]Harvard Graduate Program in Immunology, Harvard University, Boston, MA 02115, USA

[6]Department of Obstetrics and Gynecology, Weill Cornell Medical College, New York, NY 10065, USA

[7]Department of Pathology and Laboratory Medicine, Weill Cornell Medical College, New York, NY 10065, USA

SUMMARY

Dendritic cells (DCs) are required to initiate and sustain T cell-dependent anti-cancer immunity. However, tumors often evade immune control by crippling normal DC function. The endoplasmic reticulum (ER) stress response factor XBP1 promotes intrinsic tumor growth directly, but whether it also regulates the host anti-tumor immune response is not known. Here we show that constitutive activation of XBP1 in tumor-associated DCs (tDCs) drives ovarian cancer (OvCa)

*Correspondence: lglimche@med.cornell.edu.

AUTHOR CONTRIBUTIONS

J.R.C.-R. conceived, designed, and performed the research, analyzed data, and wrote the manuscript. P.C.S. performed in vitro experiments and analyzed data. M.R.R. performed in vivo experiments using p53/K-ras hosts and analyzed data. S.C. performed in vitro experiments regarding 4-HNE-protein modifications. A.P.-P. performed some nanoparticle experiments, carried out mouse surgeries, and analyzed data. M.S. performed in vitro experiments. S.Z. performed all mass spectrometry experiments and analyzed proteomics data. S.E.B. provided mouse strains, analyzed data, and wrote the manuscript. D.G., K.H., L.H.E., and T.C. performed surgeries and provided all human patient specimens described. A.-H.L. provided crucial genetic models and tools to analyze the ER stress response in vivo and in vitro. J.R.C.-G. provided OvCa models and cell lines, analyzed data, and wrote the manuscript. L.H.G. conceived and designed the research, analyzed data, and wrote the manuscript.

ACCESSION NUMBERS

The accession number for global transcription profiling data reported in this paper is National Center for Biotechnology Information (NCBI) Gene Expression Omnibus (GEO): GSE68472.

SUPPLEMENTAL INFORMATION

Supplemental Information includes Supplemental Experimental Procedures, six figures, and three tables and can be found with this article online at http://dx.doi.org/10.1016/j.cell.2015.05.025.

progression by blunting anti-tumor immunity. XBP1 activation, fueled by lipid peroxidation byproducts, induced a triglyceride biosynthetic program in tDCs leading to abnormal lipid accumulation and subsequent inhibition of tDC capacity to support anti-tumor T cells. Accordingly, DC-specific XBP1 deletion or selective nanoparticle-mediated XBP1 silencing in tDCs restored their immunostimulatory activity in situ and extended survival by evoking protective type 1 anti-tumor responses. Targeting the ER stress response should concomitantly inhibit tumor growth and enhance anti-cancer immunity, thus offering a unique approach to cancer immunotherapy.

Abstract

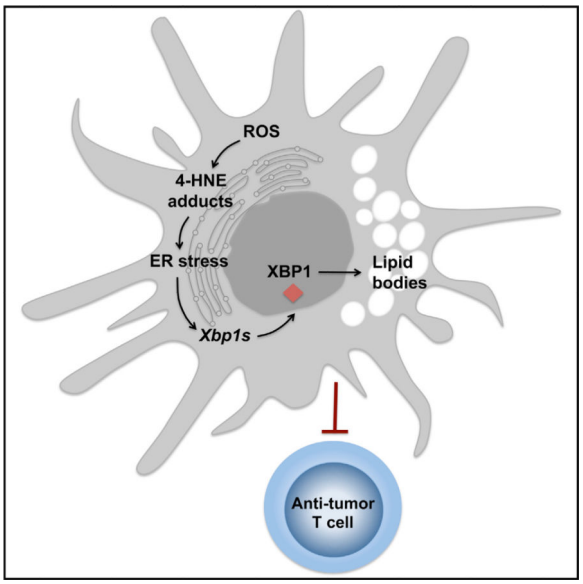

INTRODUCTION

The endoplasmic reticulum (ER) functions primarily to process newly synthesized secretory and transmembrane proteins. Abnormal accumulation of unfolded proteins in this compartment causes a state of “ER stress,” which is a hallmark feature of secretory cells and many diseases, including diabetes, neuro-degeneration, and cancer (Hetz et al., 2013). Adaptation to protein-folding stress is mediated by activation of an integrated signal transduction pathway dubbed the ER stress or unfolded protein response (UPR) that signals through three distinct stress sensors located at the ER membrane: IRE1α, ATF6, and PERK (Hetz et al., 2013). The most conserved UPR arm is IRE1α. During ER stress, this kinase oligomerizes, autophosphorylates, and uses its endoribonuclease activity to excise a 26-nucleotide fragment from the unspliced *Xbp1* mRNA (Yoshida et al., 2001) that gives rise to functional XBP1, a potent multitasking transcription factor that promotes ER chaperone expression and regulates distinct sets of target genes in a cell type-specific manner (Lee et al., 2003b; Yoshida et al., 2001).

Aggressive tumors evolve strategies to thrive in adverse conditions that induce ER stress such as hypoxia, nutrient starvation, and oxidative stress by adjusting ER protein folding

capacity (Hetz et al., 2013). In cancer cells, XBP1 confers drug resistance by preventing drug-induced cell-cycle arrest, mitochondrial permeability, and apoptosis (Gomez et al., 2007). XBP1 drives multiple myeloma (Lee et al., 2003a) and chronic lymphocytic leukemia (Tang et al., 2014). We recently demonstrated that XBP1 facilitates triple-negative breast cancer progression by promoting tumor cell survival and metastatic capacity under hypoxic conditions (Chen et al., 2014). XBP1 expression in cancer cells directly supports tumorigenesis, but whether it also creates a tumor-permissive immune milieu is unknown.

In most solid cancers, nonmalignant cells such as leukocytes, vascular cells, and fibroblasts are exposed to similarly harsh microenvironmental conditions while stimulating tumor development and progression (Whiteside, 2008). Leukocyte recruitment to established cancers has pro-tumoral effects, including secretion of growth factors that enhance tumor cell proliferation and metastasis (Coussens and Werb, 2002), the induction of tumor vascularization via paracrine mechanisms (De Palma et al., 2007), and the orchestration of immunosuppressive networks (Zou, 2005) that restrain the protective role of the scarce leukocytes with inherent anti-tumor capacity. Ovarian tumors subvert the normal activity of infiltrating dendritic cells (DCs) to inhibit the function of otherwise protective anti-tumor T cells (Curiel et al., 2003; Scarlett et al., 2012). Eliminating or “re-programming” tumor-associated DCs (tDCs) in vivo can abrogate ovarian cancer (OvCa) progression (Cubillos-Ruiz et al., 2012; Huarte et al., 2008; Scarlett et al., 2012), but the precise molecular pathways that tumors exploit in DCs to co-opt their activity remain poorly understood. Here, we uncover an unexpected role for the ER stress response factor XBP1 as a crucial driver of DC dysfunction in OvCa-bearing hosts.

RESULTS

Robust XBP1 Activation in OvCa-Associated DCs

Myeloid cells with phenotypic features of regulatory DCs commonly infiltrate ovarian tumors and promote malignant progression by preventing activation and expansion of tumor-reactive T cells (Scarlett et al., 2012). We sought to determine whether XBP1 might drive tumor growth by inhibiting DC-dependent anti-cancer immunity. Splenic and draining lymph node DCs from mice bearing aggressive primary and metastatic OvCa (Conejo-Garcia et al., 2004; Scarlett et al., 2012) showed increased splicing of *Xbp1* mRNA compared with DCs from naive hosts (Figures 1A, S1A, and S1B). However, this process was markedly enhanced in tDCs (Figures 1A and S1C–S1F). Quantitative analyses confirmed robust expression of total and spliced *Xbp1* mRNA in tDCs, compared with closely related $CD11c^{+}MHC\text{-}II^{+}CD11b^{+}$ splenic DCs (sDCs; Figure S1G) from naive or OvCa-bearing mice (Figure 1B). Consistently, tDCs had increased nuclear XBP1 protein compared with control DCs from non-tumor sites (Figure 1C). Further, marked upregulation of canonical XBP1 target genes *ERdj4* and *Sec61a1* (Acosta-Alvear et al., 2007; Lee et al., 2003b) (Figure 1D) and general ER stress response markers *Hspa5* (*BiP*) and *Ddit3* (*CHOP*) occurred only in tDCs (Figure 1E). Constitutive *Xbp1* splicing was also observed in tDCs isolated from multiple human OvCa specimens (Figures 1F, S1H, and S1I), and expression levels of ER stress markers *BiP* and *CHOP* positively correlated in these human samples (Figure 1G). Interestingly, increased *CHOP* expression in tDCs was associated with reduced

T cell infiltration in human OvCa specimens (Figure 1H), suggesting that ER-stressed DCs may regulate T cell anti-tumor responses. Hence, DCs in the OvCa microenvironment exhibit marked upregulation of ER stress response markers and robust XBP1 activation.

DC-Intrinsic XBP1 Is Required for Optimal OvCa Progression

We next developed aggressive orthotopic ovarian tumors in conditional knockout female mice lacking functional XBP1 in DCs. Genetically modified mice harboring exon 2 of *Xbp1* flanked by two *loxP* sites (Lee et al., 2008) were crossed with mice expressing Cre recombinase under control of the integrin alpha X (*Itgax*) promoter (termed CD11c-Cre) (Figures S2A–S2C) that deletes selectively in conventional DCs (Caton et al., 2007). Consistent with recent reports (Osorio et al., 2014), conditional XBP1 deletion through CD11c-controlled Cre solely affected the proportion and number of splenic $CD8a^+$ DCs (Figures S2D–S2L). The frequency of tDCs, which are mainly $CD8\alpha\text{-}^{low}$ (Figure S1E), was not altered in mice bearing orthotopic OvCa (Figures S2G–S2J), indicating that XBP1 is dispensable for DC survival in the OvCa microenvironment. However, the development of p53/K-ras-driven primary OvCa (Scarlett et al., 2012) was significantly compromised in irradiated hosts reconstituted with $XBP1^{f/f}$ CD11c-Cre donor bone marrow (BM) compared with control hosts transplanted with XBP1-sufficient ($XBP1^{f/f}$) littermate BM (Figures 2A and 2B). Tumor growth was also inhibited in mice bearing primordial p53/K-ras-driven OvCa upon intraperitoneal (i.p.) injection of XBP1-deficient, but not WT, BM-derived DCs (BMDCs) (Figures 2C and 2D). Hence, XBP1 expression in $CD11c^+$ DCs is crucial for the rapid initiation and progression of primary OvCa, and DCs devoid of XBP1 in the tumor microenvironment show enhanced capacity to restrain tumor growth.

Since the vast majority of OvCas are diagnosed at advanced stages, with disease spread throughout the peritoneal cavity, we examined how DC-localized XBP1 impacts progression of orthotopic tumors that closely recapitulate human metastatic OvCa (Conejo-Garcia et al., 2004). Notably, OvCa-bearing female mice lacking functional XBP1 in DCs demonstrated reduced peritoneal tumor burden (Figures 2E and 2F), impaired ascites accumulation (Figure 2G), and diminished tumor-induced splenomegaly (Figure 2H) compared with control ($XBP1^{f/f}$) littermates. Consequently, these hosts displayed an ~30% increase in median survival compared with control litter-mates (Figure 2I). Similar survival results were observed in $XBP1^{f/f}$ CD11c-Cre mice developing parental orthotopic ovarian tumors (Roby et al., 2000) that do not ectopically express *Defb29* and *Vegf-A* (Figure 2J). Further confirming the detrimental role of DC-intrinsic XBP1 in OvCa, implantation of malignant cells admixed with WT BMDCs markedly promoted the growth of solid ID8-based ovarian tumors, whereas XBP1-deficient BMDCs significantly impaired this process (Figures 2K and 2L). Together, these results demonstrate that XBP1 expression in DCs is necessary for the accelerated and aggressive progression of primary and metastatic OvCas in three preclinical models of disease.

Byproducts of Lipid Peroxidation Trigger ER Stress in DCs

Constitutive XBP1 activation in tDCs suggested that cancer-derived factors in the tumor microenvironment might trigger ER stress in innate immune cells to blunt anti-tumor immunity. Interestingly, neither tumorigenic/immunosuppressive cytokines commonly

enriched at tumor sites nor hypoxia-mimicking conditions caused robust XBP1 activation in naive DCs (Figures S3A–S3C). Abnormal intracellular accumulation of peroxidized lipids is a common feature of dysfunctional DCs infiltrating several human and murine cancers (Herber et al., 2010; Ramakrishnan et al., 2014). Intracellular lipid oxidation by reactive oxygen species (ROS) generates multiple reactive byproducts such as the unsaturated aldehyde 4-hydroxy-*trans*-2-nonenal (4-HNE), shown to induce protein-folding stress by forming stable adducts with ER-resident chaperones (Vladykovskaya et al., 2012). Hence, we hypothesized that this diffusible and highly reactive aldehyde (Uchida et al., 1999) might trigger ER stress in tDCs. OvCa-associated DCs demonstrated significantly higher amounts of intracellular lipids and augmented ROS levels in comparison with control sDCs isolated from the same host or from naive mice (Figures 3A and 3B). Consistent with active lipid peroxidation, we found intracellular 4-HNE-protein adducts in tDCs isolated from human and mouse tumors (Figure 3C), and increased levels of this aldehyde were present in tDCs compared with sDC of OvCa-bearing mice (Figure 3D). Extracellular 4-HNE was not enriched in cell-free ascites or serum from OvCa-bearing hosts (Figures S3D and S3E), suggesting that this reactive aldehyde is mostly generated intracellularly due to the high lipid and ROS content in tDCs (Figures 3A and 3B). Indeed, naive sDCs exposed to cell-free OvCa ascites rapidly generated intra-cellular 4-HNE-protein adducts in a dose-dependent manner (Figure 3E). Proteomic analyses confirmed the presence of several intracellular proteins modified by the endogenous 4-HNE generated in naive DCs exposed to OvCa ascites super-natants, but not in control untreated DCs (Table S1). Of note, ascites-induced 4-HNE modified key ER-resident chaperones such as Grp78/BiP and ERdj3/Dnajb11 (Figures 3F and 3G). Induction of 4-HNE-protein adducts by ascites was inhibited when DCs were treated with the ROS-scavenging agent vitamin E or with hydralazine (Figure 3H), a hydrazine derivative (Figure S3F) previously shown to sequester reactive lipid peroxidation byproducts (Galvani et al., 2008). Treatment of freshly isolated tDCs with either vitamin E or hydralazine inhibited *Xbp1* splicing and prevented induction of general ER stress response markers triggered by ascites exposure (Figures 3I and 3J). Further, induction of *Xbp1* splicing and upregulation of ER stress response markers was observed in naive sDC exposed to 4-HNE concentrations generating intracellular adduct levels similar to those generated upon incubation with cell-free ascites (Figures S3G–S3I). Together, these data indicate that lipid peroxidation byproducts, abundant in OvCa tDCs, promote ER stress and constitutive XBP1 activation.

Constitutive XBP1 Activation Disrupts DC Homeostasis

Transcriptional profiling of WT versus XBP1-deficient DCs in OvCa ascites identified 416 significantly downregulated and 237 significantly upregulated genes (Table S2). These altered gene subsets were analyzed to identify transcriptional regulators that may explain the observed mRNA changes. Several predicted regulators were identified (Figure S4A), and XBP1, as expected, was a key node in the most highly represented gene network emerging from this analysis (Figure S4B). Interestingly, gene networks regulated by the immunosuppressive transforming growth factor-β (TGF-β), but not TGF-β itself, were suppressed in XBP1-deficient tDCs (Figure S4A). Multiple known XBP1 and UPR target genes (Acosta-Alvear et al., 2007; Lee et al., 2003b) were markedly repressed in XBP1-deficient tDCs (Figure 4A), confirming sustained ER stress in DCs infiltrating OvCa.

Expression of known regulated IRE1α-dependent decay (RIDD) target mRNAs (Hetz et al., 2013; Hollien et al., 2009; Osorio et al., 2014) was unchanged between WT and XBP1-deficient tDCs (Figure S4C), ruling out IRE1α artificial overactivation due to absence of functional XBP1. We found four significantly enriched functional categories, including carbohydrate and lipid metabolic processes, protein localization and transport, and regulation of cell communication (Figure S4D). Of particular interest, tDCs devoid of XBP1 displayed marked downregulation of multiple genes involved in lipid metabolic pathways and especially, in triglyceride biosynthesis (Figure 4B). Given the strong association between excessive lipid accumulation and DC dysfunction in cancer (Herber et al., 2010; Ramakrishnan et al., 2014), we investigated XBP1 as a potential mediator of this process. Consistent with sustained ER stress at tumor locations, OvCa-associated DCs exhibited marked upregulation of multiple XBP1-controlled triglyceride biosynthetic genes (Figure 4B), including *Agpat6*, *Fasn*, *Scd2*, and *Lpar1* (Figure S5A), and these genes were rapidly induced in naive sDCs exposed to 4-HNE (Figure S5B). OvCa-infiltrating DCs lacking XBP1 showed reduced intracellular lipid content compared with WT tDCs (Figure 4C) and displayed a marked decrease in the number of cytosolic lipid droplets (Figures 4D and 4E), as well as reduced intracellular levels of total triglycerides (Figure 4F). Other lipid classes were unaffected (Figure S5C), and these observations were confirmed by analyzing cell-free ascites supernatants (Figure S5D). Decreased intracellular lipid content in XBP1-deficient tDCs was not due to defective expression of genes encoding scavenger receptors (*Cd36*, *Cd68*, *Msr1*) implicated in extracellular lipid uptake (Figure S5E). Notably, exposure to cell-free OvCa ascites augmented the intracellular lipid content of mouse tDCs and was prevented by concurrent treatment with TOFA, an inhibitor of fatty acid synthesis (Figures 4G and S5F). Pharmacological inhibition of IRE1α/XBP1 activation using the IRE1α inhibitor 4μ8c also reduced ascites-driven lipid biogenesis in tDCs (Figures 4G and S5F). Consistent with ROS as key generators of XBP1-activating 4-HNE (Figure 3), treatment of tDCs with the global ROS scavenger vitamin E, but not with the superoxide-specific scavenger Tiron reduced intracellular lipid content (Figures 4G and S5F). Further, sequestering intracellular 4-HNE using hydralazine also prevented ascites-induced lipid biogenesis in tDCs (Figure S5G). Taken together, the transcriptomic and functional data indicate that sustained activation of XBP1 disrupts intracellular lipid homeostasis in OvCa-associated DCs.

XBP1-Deficient tDCs Support T Cell Activation

Aberrant lipid accumulation by tDCs obstructs their normal antigen-presenting capacity, ultimately blunting anti-tumor im mune responses (Herber et al., 2010; Ramakrishnan et al., 2014). T cells are the sole immune population that exerts significant pressure against OvCa, and the magnitude of intra-tumoral T cell infiltration strongly correlates with better outcome in OvCa patients (Curiel et al., 2003; Zhang et al., 2003). Hence XBP1-deficient tDCs with reduced intracellular lipids might support rather than repress T cell activation and function at tumor sites. Incubation of BMDCs in tumor-conditioned media (TCM) induced *Xbp1* splicing (Figure S6A) and subsequent triglyceride accumulation (Figure S6B), leading to decreased surface expression of MHC-I complexes loaded with intracellularly processed peptide (ovalbumin [OVA]-derived SIINFEKL) (Figure S6C). Accordingly, BMDCs pulsed with full-length OVA protein in the presence of TCM compared with normal culture media

had reduced capacity to induce OT-1 T cell proliferation (Figure 5A). This impairment was also observed upon incubation with the ER stressor tunicamycin or by enforcing lipid accumulation using oleate during antigen loading (Figure 5A). In contrast, XBP1-deficient BMDCs unable to accumulate triglycerides upon TCM exposure (Figure S6B) did not show significant reduction in surface levels of peptide-loaded MHC-I complexes when pulsed under this condition (Figure S6C). This effect was not due to enhanced OVA cleavage (Figure S6D) or increased expression of MHC-I by XBP1-deficient BMDCs (Figure S6E). Consequently, BMDCs lacking XBP1 demonstrated enhanced capacity to induce the proliferation of OT-1 T cells when pulsed with OVA under TCM, compared with their WT counterparts pulsed likewise (Figure 5B).

XBP1-deficient tDCs pulsed with full-length OVA or apoptotic OVA-expressing tumor cells in the presence of ascites also had enhanced capacity to induce OT-1 T cell expansion, compared with WT tDCs (Figures 5C and S6F–S6H), and these differences were not due to reduced PD-L1 expression by XBP1-deficient tDC (Figure S6I). Consistent with impaired lipid accumulation upon global ROS scavenging and IRE1α/1 inhibition (Figure 4G), pre-treatment of WT tDC with vitamin E phenocopied the improved antigen-presenting capacity of XBP1-deficient tDCs (Figure 5C). Further supporting the enhanced function of XBP1-deficient DCs at tumor locations, p53/K-ras ovarian tumors developed in irradiated hosts reconstituted with $XBP1^{f/f}$ CD11c-Cre BM (Figure 2A) demonstrated an ~7-fold increase in the levels of intratumoral T cell infiltration compared with tumors developed in mice reconstituted with WT BM (Figure S6J). Most of these $CD4^+$ T cells were antigen experienced ($CD44^+$), and a significant proportion expressed the Th1-polarizing transcription factor T-bet (Figure S6K). The majority of $CD8^+$ T cells present in p53/K-ras tumors generated in XBP1-deficient hosts also expressed CD44 and a proportion of those produced Granzyme B in situ (Figure S6L). Reduced PD-1 levels were observed on these cells compared with the few $CD8^+$ T cells poorly infiltrating p53/K-ras tumors developed in mice reconstituted with WT BM (Figure S6M). While PD-1 levels remained unaltered on peritoneal T cells in $XBP1^{f/f}$ or $XBP1^{f/f}$ CD11c-Cre mice harboring metastatic ID8-based OvCa (Figure S6N), the latter demonstrated a marked increase in the proportion of infiltrating $CD44^+IFN\gamma$-secreting $CD8^+$ and $CD4^+$ T cells at tumor sites (Figures 5D and 5E). In addition, the proportion of $Foxp3^+$ T regulatory cells infiltrating tumor locations was significantly lower in XBP1-deficient hosts (Figure 5F). To functionally demonstrate that the enhanced activity of XBP1-deficient DCs in OvCa results in improved T cell-mediated anti-tumor responses, orthotopic ovarian tumors were developed in WT or XBP1-deficient hosts, and T cells were obtained from spleens and draining lymph nodes 30 days after tumor implantation. Isolated T cells were independently transferred into naive mice, and hosts were then challenged with ovarian tumors in the flank. Notably, T cells obtained from tumor-bearing mice lacking XBP1 in DCs demonstrated improved capacity to restrain tumor growth in adoptively transferred hosts, compared with untreated mice or control mice receiving T cells isolated from WT OvCa-bearing mice (Figures 5G and 5H). Together, these data indicate that constitutive XBP1 activation promotes anti-tumor immune tolerance by OvCa-associated DCs.

Therapeutic XBP1 Silencing in tDCs Extends Host Survival by Inducing Anti-tumor Immunity

Silencing XBP1 expression in OvCa-associated DCs could potentially restore their immunogenic attributes in situ to promote the function of infiltrating anti-tumor T cells. To selectively target XBP1 in tDCs, we utilized our previously optimized system of polyethylenimine (PEI)-based nanoparticles encapsulating siRNA (Cubillos-Ruiz et al., 2009, 2012). These nanocomplexes are preferentially and avidly engulfed by abundant phagocytic tDCs upon i.p. injection, enabling selective in vivo gene silencing. Also, PEI-based nanoparticles inherently activate OvCa-associated DCs by triggering TLR signaling that induces potent immunoadjuvant activity against tumors (Cubillos-Ruiz et al., 2009). Confirming previous findings, nanoparticles were selectively taken up by tDCs present in malignant ascites of mice bearing metastatic OvCa (Figure S7A). PEI-based nanocomplexes delivering *Xbp1*-specific siRNA induced ~65% gene silencing in target tDC compared with control luciferase-targeting siRNA nanoparticles (Figure S7B). The functional effects of gene silencing were confirmed by the decreased expression of the canonical XBP1 targets *EDEM* and *Sec61a1*, as well as lipid biosynthesis-related *Agpat6 and Scd2* in tDCs (Figure S6C). Further, tDCs isolated from mice treated with either XBP1- or IRE1α-targeting nanoparticles demonstrated reduced triglyceride levels compared with control tDCs (Figure S7D), and the in vivo proliferation of adoptively transferred CFSE-labeled OT-1 T cells in the OvCa microenvironment was significantly enhanced in mice pulsed i.p. with full-length OVA protein when XBP1 expression was specifically silenced in tDCs (Figures 6A–6C). Therapeutic administration of *Xbp1*-silencing nanocomplexes reduced the number of metastatic cancer cells in the peritoneal cavity (Figure 6D) and diminished malignant ascites accumulation (Figure 6E). These effects occurred concomitantly with enhanced infiltration of endogenous antigen-experienced/ activated T cells at tumor locations compared with control nano-particles (Figure 6F). Indeed, silencing XBP1 expression in tDCs markedly enhanced the capacity of infiltrating T cells to respond to tumor antigens, as evidenced by ex vivo interferon-γ (IFN-γ) and Granzyme B secretion using BMDCs pulsed with tumor antigens (Figure 6G). Splenic T cells isolated from mice treated with XBP1-silencing nanocomplexes also demonstrated improved responses upon exposure to tumor antigens in similar re-call assays (Figure 6H), indicating development of enhanced anti-tumor memory responses. These data reinforce the concept that abrogating XBP1 function in tDCs enables the activation and expansion of endogenous anti-tumor T cells in vivo.

To determine whether abrogation of the IRE1α/XBP1 pathway selectively in tDCs had significant therapeutic effects, mice bearing aggressive orthotopic ovarian tumors were i.p. treated with saline, non-targeting or gene-specific siRNA-PEI nanocomplexes. Treatments started 12 days after tumor implantation, and injections were administered every 4 days for a period of 3 weeks. Interestingly, WT mice treated with either XBP1- or IRE1α-silencing nanoparticles demonstrated a marked increase in survival compared with control groups, reinforcing dependence of this phenotype on spliced *Xbp1* rather than RIDD (Figure 7A). However, *Rag2*-deficient hosts bearing ovarian tumors were unable to respond to this treatment, demonstrating that an intact adaptive immune system is necessary for the observed therapeutic benefit (Figure 7B). Together, these data indicate that targeting the

IRE1α/XBP1 branch of the ER stress response in tDCs induces protective immune responses against OvCa.

DISCUSSION

Here we uncover an unexpected role for the ER stress response factor XBP1 as a central driver of DC malfunction in the tumor microenvironment. Our findings suggest a strategy whereby a lethal cancer exploits the most conserved arm of the ER stress response in tumor-resident DCs to disrupt their homeostasis, alter their local antigen-presenting capacity, and ultimately evade T cell-mediated immune control. While the ER stress response, and especially XBP1 activation, was previously shown to promote tumorigenesis, we now propose that this integrated cellular pathway further supports malignant progression by inhibiting the development of protective anti-tumor immunity via manipulation of normal DC function.

Gabrilovich and colleagues have elegantly demonstrated that cancer-associated DCs accumulate substantial amounts of oxidized lipids that diminish their antigen-presenting ability (Herber et al., 2010; Ramakrishnan et al., 2014). Our transcriptional and functional analyses suggest that XBP1 plays a crucial role in promoting aberrant lipid accumulation by dysfunctional tDCs and that lipid peroxidation byproducts, like 4-HNE, sustain ER stress and fuel constitutive XBP1 activation in tDCs. Interestingly, 4-HNE was shown to induce the UPR in endothelial cells by forming covalent adducts with ER resident chaperones, thereby promoting vascular inflammation and atherosclerosis (Vladykovskaya et al., 2012). Consistent with previous reports linking XBP1 and lipid biosynthesis (Lee et al., 2008; Sriburi et al., 2004), we found that enhanced intracellular lipid accumulation by tDCs required ROS generation and IRE1α/XBP1 activation. Interestingly, exposure to 4-HNE is sufficient for promoting fat accumulation in worms and mice (Singh et al., 2008, 2009). Other lipid peroxidation byproducts like acrolein, malondialdehyde, and 4-hydroxyhexenal form stable adducts with cellular proteins (Negre-Salvayre et al., 2008), suggesting that they might also induce immunosuppression in the tumor microenvironment by triggering ER stress in infiltrating innate immune cells. Further, chemotherapeutic agents are known to induce oxidative stress and subsequent 4-HNE generation (Velez et al., 2011), suggesting that chemotherapy might promote “tumorigenic ER stress” in cells of the tumor microenvironment. This is particularly relevant to OvCa, as patients diagnosed with this disease show persistent, refractory, or recurrent cancer following treatment with surgery and first-line chemotherapy. Notably, the status of lipid peroxidation at the time of tumor removal has been suggested as a putative marker of disease recurrence in breast cancer patients (Herrera et al., 2014).

Our findings suggest a model in which reactive metabolic byproducts induced by the tumor microenvironment, like 4-HNE, can initiate and sustain pro-tumorigenic ER stress in infiltrating tDCs. Constitutive activation of the IRE1α/XBP1 arm through this process disrupts global tDC homeostasis and consequently inhibits tDC capacity to locally support T cell-mediated anti-tumor responses. Since splenic and draining lymph node DCs of OvCa mice also showed increased levels of *Xbp1s* compared with naive hosts, it is reasonable to

consider that XBP1 might also regulate anti-tumor immunity by operating in DCs residing in lymphoid organs that may have migrated from the primary tumor site.

Activating T cell immunity to eliminate tumor cells is the most promising anti-cancer strategy since the development of chemotherapy, as demonstrated by the shrinkage of melanoma in response to checkpoint blockers. Further, adoptively transferred anti-tumor T cells (expanded from tumor specimens or genetically manipulated) can elicit robust and long-lasting anti-tumor responses (Bollard et al., 2007; Morgan et al., 2006). How ever, in most cases, the optimal cytotoxic activity of such tumor-reactive T cells is drastically reduced precisely because cancer-associated DCs are unable to support T cell function (Curiel et al., 2003; Scarlett et al., 2012). Our results reveal that DC-specific deletion of XBP1 can extend host survival by converting immunosuppressive tDCs into activators of type 1 immunity in OvCa-infiltrating T cells. Indeed, therapeutic silencing of XBP1 in tDCs using siRNA-encapsulating nanocarriers reversed their immunosuppressive phenotype and prolonged host survival by inducing protective anti-tumor immune responses. Novel and more effective therapeutic strategies are urgently needed to improve the dismal prognosis of patients with meta-static OvCa and other lethal cancers. Our study demonstrates the feasibility and immunotherapeutic potential of targeting ER stress-driven XBP1 selectively in tDCs using a nanotechnology-based system that may slow or prevent the usually inevitable recurrence observed in OvCa patients who have been “optimally” debulked. Targeting IRE1α/XBP1 signaling in cancer-bearing hosts with small molecule IRE1α inhibitors could induce two parallel, mutually reinforcing anti-tumor mechanisms: the direct inhibition of cancer cell survival and the simultaneous induction of protective anti-tumor immunity.

EXPERIMENTAL PROCEDURES

Tissues, Mice, and Cell Lines

Stages III–IV human OvCa specimens and malignant ascites samples were procured through Surgical Pathology at Weill Cornell under an approved protocol where research samples remained unidentified. Tumor single-cell suspensions were generated as described (Conejo-Garcia et al., 2004). Malignant peritoneal ascites samples from patients with metastatic OvCa were centrifuged for 10 min at 1,300 rpm, and red blood cells were lysed prior to fluorescence-activated cell sorting (FACS) analysis. Mice were housed at the animal facilities of Harvard School of Public School, Weill Cornell, or The Wistar Institute. Our Institutional Animal Care and Use Committees approved all animal experiments described in this study. Transgenic mouse strains and tumor models used are described in the Supplemental Experimental Procedures.

Isolation of Human and Mouse DCs

Human patient OvCa-associated DCs ($CD45^+CD3^-$ $CD20^-$ $CD11c^+DEC205^+$) were sorted from tumor single-cell suspensions or malignant ascites using flow cytometry, following the gating strategy in Figure S1. During sorting, viable cells were identified using the LIVE/DEAD Fixable Yellow Dead Cell Stain Kit (Life Technologies). Mouse OvCa-associated DCs ($CD45^+CD11c^+$ $CD11b^+MHC\text{-}II^+CD8a^{low}$) were sorted from single-cell suspensions

of p53/K-ras-driven ovarian tumors or from peritoneal wash (10 ml 1 × 3 PBS) or malignant ascites samples from mice bearing aggressive ID8-*Defb29/Vegf-A* i.p. OvCa, per gating strategy (Figure S1). All fluorescently labeled antibodies were from BioLegend. Control sDCs ($CD45^+CD11c^+CD11b^+MHC\text{-}II^+CD8\alpha^-$) were FACS sorted from spleens of naive or OvCa-bearing mice using Collagenase D and DNase I treatment followed by incubation with the indicated antibodies. In all cases, BMDCs were generated from naive $XBP1^{f/f}$ (WT) or $XBP1^{f/f}$ CD11c-Cre (XBP1 deficient) BM via incubation in media supplemented with 20 ng/ml recombinant granulocyte macrophage colony-stimulating factor (GMCSF) (Gemini) (Scarlett et al., 2012). Cells were harvested at day 7 of expansion and used directly for subsequent in vitro or in vivo functional assays.

Reagents and In Vitro Cellular Treatments

Murine recombinant cytokines were purchased from Peprotech. Cobalt chlo-ride (10–100 μM), tunicamycin (1 μg/ml), Tiron (100–500 μM), vitamin E (α-tocopherol, 50–100 μM) and hydralazine (100 μg/ml) were from Sigma. 2′,7′-dichlorofluorescin diacetate (DCFDA) staining was utilized for intracellular ROS detection (Abcam). Purified 4-HNE (Cayman Chemical) and 4-HNE-protein adducts in ascites samples and DCs were detected and quantified through competitive ELISA (Cell Biolabs). 5-tetradecyl-oxy-2-furoic acid (TOFA) (Cayman Chemical) was used at a final concentration of 5 μg/ml to inhibit fatty acid synthesis in DCs. The IRE1α-specific inhibitor 4μ8c (Millipore) was used at 10 μM and DQ-OVA (Invitrogen) at 50 μg/ml. Cell-free (0.22 mmfiltered) TCM was harvested from ID8-*Defb29/Vegf-A* OvCa cells grown to confluency in complete Dulbecco's modified Eagle's medium (DMEM) supplemented with 10% fetal bovine serum (FBS).

RNA-seq and DC Transcriptional Profile

tDCs were sorted from peritoneal wash samples of $XBP1^{f/f}$ or $XBP1^{f/f}$ CD11c-Cre female mice (n = 3 per group) bearing aggressive ID8-*Defb29/Vegf-A* ovarian tumors for 3 weeks. Total RNA was isolated using the miRVANA miRNA isolation Kit (Life Technologies), further concentrated via RNeasy MinElute columns (QIAGEN) and RNA quality and integrity confirmed in an Agilent Bioanalyzer 2100. In all cases, RINs were 9.50 or higher. mRNA libraries were generated and sequenced at the Weill Cornell Epigenomics Facility. All primers used in this study are described in Table S3; Supplemental Information for details.

Flow Cytometry and Lipid Staining

Intracellular lipid content was evaluated via flow cytometry using 4,4-Difluoro-1,3,5,7,8-Pentamethyl-4-Bora-3a,4a-Diaza-*s*-Indacene (BODIPY 493/503; Life Technologies) (Herber et al., 2010). Briefly, 5×10^6 splenic or malignant peritoneal wash cells were stained for surface markers using antibodies that do not overlap with BODIPY 493/503, namely CD11c-APC, CD45-APC-Cy7, and CD11b-Pacific Blue, followed by staining with 500 μl of BODIPY 493/503 at 0.5 μg/ml in PBS for 15 min at room temperature in the dark. BODIPY 493/503 staining was detected in the PE channel. For intracellular cytokine staining, 5×10^6 cells from malignant peritoneal wash samples were stimulated for 6 hr in 10% FBS complete RPMI containing phorbol myristate acetate (PMA), Ionomycin

(Calbiochem), and Brefeldin A (BioLegend). Cells were collected and stained for surface markers and intracellular cytokines (BioLegend) according to Foxp3/Transcription Factor Staining buffer set (eBioscience). Flow cytometry was performed on a LSRII instrument (BD Biosciences). Cell populations were sorted from peritoneal washes of OvCa-bearing mice or human ascites or tumor single-cell suspensions with a FACSAria sorter (BD Biosciences), and flow cytometry data were analyzed using FlowJo v.9 or v.10.

Statistical Analysis

Unless noted otherwise, all experiments were repeated at least two times and results were similar between repeats. Animal experiments used between three and six mice per group; $p < 0.05$ was considered to be statistically significant. All statistical analyses were done using Graph Pad Prism 5.0. Differences between the means of experimental groups were calculated using a two-tailed unpaired Student's t test. Error bars represent SEM from independent samples assayed within the represented experiments. Survival rates were compared using the log-rank test. All survival experiments used at least six mice per group. This number provides a 5% significance level and 95% power to detect differences in survival of 20% or greater.

Supplementary Material

Refer to Web version on PubMed Central for supplementary material.

ACKNOWLEDGMENTS

This study was supported by NIH grants R01CA112663 to L.H.G., R01CA157664 and R01CA124515 to J.R.C.-G., and 1S10RR025449-01 to S.Z. J.R.C.-R. was supported by the Irvington Institute Fellowship Program of the Cancer Research Institute. A.P.-P. was supported by Fundación Alfonso Martín Escudero. We thank all members of the WCMC Epigenomics Core Facility for excellent assistance with NGS, J. Wickramasinghe and A. Kosenkov at the Bioinformatics Facility of TWI for outstanding computational biology support, and J. McCormick at WCMC for expert flow cytometry assistance. We also thank Diana K. Morales, Andres Cubillos-Ruiz, and the members of the Glimcher laboratory for helpful suggestions and critical reading of this manuscript. L.H.G. holds equity in and is on the board of directors of Bristol-Myers-Squibb.

REFERENCES

Acosta-Alvear D, Zhou Y, Blais A, Tsikitis M, Lents NH, Arias C, Lennon CJ, Kluger Y, Dynlacht BD. XBP1 controls diverse cell type- and condition-specific transcriptional regulatory networks. Mol. Cell. 2007; 27:53–66. [PubMed: 17612490]

Bollard CM, Gottschalk S, Leen AM, Weiss H, Straathof KC, Carrum G, Khalil M, Wu MF, Huls MH, Chang CC, et al. Complete responses of relapsed lymphoma following genetic modification of tumor-antigen presenting cells and T-lymphocyte transfer. Blood. 2007; 110:2838–2845. [PubMed: 17609424]

Caton ML, Smith-Raska MR, Reizis B. Notch-RBP-J signaling controls the homeostasis of CD8- dendritic cells in the spleen. J. Exp. Med. 2007; 204:1653–1664. [PubMed: 17591855]

Chen X, Iliopoulos D, Zhang Q, Tang Q, Greenblatt MB, Hatziapostolou M, Lim E, Tam WL, Ni M, Chen Y, et al. XBP1 promotes triple-negative breast cancer by controlling the HIF1α pathway. Nature. 2014; 508:103–107. [PubMed: 24670641]

Conejo-Garcia JR, Benencia F, Courreges MC, Kang E, Mohamed-Hadley A, Buckanovich RJ, Holtz DO, Jenkins A, Na H, Zhang L, et al. Tumor-infiltrating dendritic cell precursors recruited by a beta-defensin contribute to vasculogenesis under the influence of Vegf-A. Nat. Med. 2004; 10:950–958. [PubMed: 15334073]

Coussens LM, Werb Z. Inflammation and cancer. Nature. 2002; 420:860–867. [PubMed: 12490959]

Cubillos-Ruiz JR, Engle X, Scarlett UK, Martinez D, Barber A, Elgueta R, Wang L, Nesbeth Y, Durant Y, Gewirtz AT, et al. Polyethylenimine-based siRNA nanocomplexes reprogram tumor-associated dendritic cells via TLR5 to elicit therapeutic antitumor immunity. J. Clin. Invest. 2009; 119:2231–2244. [PubMed: 19620771]

Cubillos-Ruiz JR, Baird JR, Tesone AJ, Rutkowski MR, Scarlett UK, Camposeco-Jacobs AL, Anadon-Arnillas J, Harwood NM, Korc M, Fiering SN, et al. Reprogramming tumor-associated dendritic cells in vivo using miRNA mimetics triggers protective immunity against ovarian cancer. Cancer Res. 2012; 72:1683–1693. [PubMed: 22307839]

Curiel TJ, Wei S, Dong H, Alvarez X, Cheng P, Mottram P, Krzysiek R, Knutson KL, Daniel B, Zimmermann MC, et al. Blockade of B7-H1 improves myeloid dendritic cell-mediated antitumor immunity. Nat. Med. 2003; 9:562–567. [PubMed: 12704383]

De Palma M, Murdoch C, Venneri MA, Naldini L, Lewis CE. Tie2-expressing monocytes: regulation of tumor angiogenesis and therapeutic implications. Trends Immunol. 2007; 28:519–524. [PubMed: 17981504]

Galvani S, Coatrieux C, Elbaz M, Grazide MH, Thiers JC, Parini A, Uchida K, Kamar N, Rostaing L, Baltas M, et al. Carbonyl scavenger and antiatherogenic effects of hydrazine derivatives. Free Radic. Biol. Med. 2008; 45:1457–1467. [PubMed: 18801426]

Gomez BP, Riggins RB, Shajahan AN, Klimach U, Wang A, Crawford AC, Zhu Y, Zwart A, Wang M, Clarke R. Human X-box binding protein-1 confers both estrogen independence and antiestrogen resistance in breast cancer cell lines. FASEB J. 2007; 21:4013–4027. [PubMed: 17660348]

Herber DL, Cao W, Nefedova Y, Novitskiy SV, Nagaraj S, Tyurin VA, Corzo A, Cho HI, Celis E, Lennox B, et al. Lipid accumulation and dendritic cell dysfunction in cancer. Nat. Med. 2010; 16:880–886. [PubMed: 20622859]

Herrera AC, Victorino VJ, Campos FC, Verenitach BD, Lemos LT, Aranome AM, Oliveira SR, Cecchini AL, Simão AN, Abdelhay E, et al. Impact of tumor removal on the systemic oxidative profile of patients with breast cancer discloses lipid peroxidation at diagnosis as a putative marker of disease recurrence. Clin. Breast Cancer. 2014; 14:451–459. [PubMed: 25077997]

Hetz C, Chevet E, Harding HP. Targeting the unfolded protein response in disease. Nat. Rev. Drug Discov. 2013; 12:703–719. [PubMed: 23989796]

Hollien J, Lin JH, Li H, Stevens N, Walter P, Weissman JS. Regulated Ire1-dependent decay of messenger RNAs in mammalian cells. J. Cell Biol. 2009; 186:323–331. [PubMed: 19651891]

Huarte E, Cubillos-Ruiz JR, Nesbeth YC, Scarlett UK, Martinez DG, Buckanovich RJ, Benencia F, Stan RV, Keler T, Sarobe P, et al. Depletion of dendritic cells delays ovarian cancer progression by boosting antitumor immunity. Cancer Res. 2008; 68:7684–7691. [PubMed: 18768667]

Lee AH, Iwakoshi NN, Anderson KC, Glimcher LH. Proteasome inhibitors disrupt the unfolded protein response in myeloma cells. Proc. Natl. Acad. Sci. USA. 2003a; 100:9946–9951. [PubMed: 12902539]

Lee AH, Iwakoshi NN, Glimcher LH. XBP-1 regulates a subset of endoplasmic reticulum resident chaperone genes in the unfolded protein response. Mol. Cell. Biol. 2003b; 23:7448–7459. [PubMed: 14559994]

Lee AH, Scapa EF, Cohen DE, Glimcher LH. Regulation of hepatic lipogenesis by the transcription factor XBP1. Science. 2008; 320:1492–1496. [PubMed: 18556558]

Morgan RA, Dudley ME, Wunderlich JR, Hughes MS, Yang JC, Sherry RM, Royal RE, Topalian SL, Kammula US, Restifo NP, et al. Cancer regression in patients after transfer of genetically engineered lymphocytes. Science. 2006; 314:126–129. [PubMed: 16946036]

Negre-Salvayre A, Coatrieux C, Ingueneau C, Salvayre R. Advanced lipid peroxidation end products in oxidative damage to proteins. Potential role in diseases and therapeutic prospects for the inhibitors. Br. J. Pharmacol. 2008; 153:6–20. [PubMed: 17643134]

Osorio F, Tavernier SJ, Hoffmann E, Saeys Y, Martens L, Vetters J, Delrue I, De Rycke R, Parthoens E, Pouliot P, et al. The unfolded-protein-response sensor IRE-1α regulates the function of CD8α+ dendritic cells. Nat. Immunol. 2014; 15:248–257. [PubMed: 24441789]

Ramakrishnan R, Tyurin VA, Veglia F, Condamine T, Amoscato A, Mohammadyani D, Johnson JJ, Zhang LM, Klein-Seetharaman J, Celis E, et al. Oxidized lipids block antigen cross-presentation by dendritic cells in cancer. J. Immunol. 2014; 192:2920–2931. [PubMed: 24554775]

Roby KF, Taylor CC, Sweetwood JP, Cheng Y, Pace JL, Tawfik O, Persons DL, Smith PG, Terranova PF. Development of a syngeneic mouse model for events related to ovarian cancer. Carcinogenesis. 2000; 21:585–591. [PubMed: 10753190]

Scarlett UK, Rutkowski MR, Rauwerdink AM, Fields J, Escovar-Fadul X, Baird J, Cubillos-Ruiz JR, Jacobs AC, Gonzalez JL, Weaver J, et al. Ovarian cancer progression is controlled by phenotypic changes in dendritic cells. J. Exp. Med. 2012; 209:495–506. [PubMed: 22351930]

Singh SP, Niemczyk M, Saini D, Awasthi YC, Zimniak L, Zimniak P. Role of the electrophilic lipid peroxidation product 4-hydroxynonenal in the development and maintenance of obesity in mice. Biochemistry. 2008; 47:3900–3911. [PubMed: 18311940]

Singh SP, Niemczyk M, Zimniak L, Zimniak P. Fat accumulation in Caenorhabditis elegans triggered by the electrophilic lipid peroxidation product 4-hydroxynonenal (4-HNE). Aging. 2009; 1:68–80. [PubMed: 20157589]

Sriburi R, Jackowski S, Mori K, Brewer JW. XBP1: a link between the unfolded protein response, lipid biosynthesis, and biogenesis of the endoplasmic reticulum. J. Cell Biol. 2004; 167:35–41. [PubMed: 15466483]

Tang CH, Ranatunga S, Kriss CL, Cubitt CL, Tao J, Pinilla-Ibarz JA, Del Valle JR, Hu CC. Inhibition of ER stress-associated IRE-1/XBP-1 pathway reduces leukemic cell survival. J. Clin. Invest. 2014; 124:2585–2598. [PubMed: 24812669]

Uchida K, Shiraishi M, Naito Y, Torii Y, Nakamura Y, Osawa T. Activation of stress signaling pathways by the end product of lipid peroxidation. 4-hydroxy-2-nonenal is a potential inducer of intracellular peroxide production. J. Biol. Chem. 1999; 274:2234–2242. [PubMed: 9890986]

Velez JM, Miriyala S, Nithipongvanitch R, Noel T, Plabplueng CD, Oberley T, Jungsuwadee P, Van Remmen H, Vore M, St Clair DK. p53 Regulates oxidative stress-mediated retrograde signaling: a novel mechanism for chemotherapy-induced cardiac injury. PLoS ONE. 2011; 6:e18005. [PubMed: 21479164]

Vladykovskaya E, Sithu SD, Haberzettl P, Wickramasinghe NS, Merchant ML, Hill BG, McCracken J, Agarwal A, Dougherty S, Gordon SA, et al. Lipid peroxidation product 4-hydroxy-trans-2-nonenal causes endothelial activation by inducing endoplasmic reticulum stress. J. Biol. Chem. 2012; 287:11398–11409. [PubMed: 22228760]

Whiteside TL. The tumor microenvironment and its role in promoting tumor growth. Oncogene. 2008; 27:5904–5912. [PubMed: 18836471]

Yoshida H, Matsui T, Yamamoto A, Okada T, Mori K. XBP1 mRNA is induced by ATF6 and spliced by IRE1 in response to ER stress to produce a highly active transcription factor. Cell. 2001; 107:881–891. [PubMed: 11779464]

Zhang L, Conejo-Garcia JR, Katsaros D, Gimotty PA, Massobrio M, Regnani G, Makrigiannakis A, Gray H, Schlienger K, Liebman MN, et al. Intratumoral T cells, recurrence, and survival in epithelial ovarian cancer. N. Engl. J. Med. 2003; 348:203–213. [PubMed: 12529460]

Zou W. Immunosuppressive networks in the tumour environment and their therapeutic relevance. Nat. Rev. Cancer. 2005; 5:263–274. [PubMed: 15776005]

Highlights

- DCs in the tumor microenvironment exhibit ER stress and robust IRE1α/XBP1 activation
- DC-intrinsic XBP1 drives primary and metastatic ovarian cancer progression
- XBP1 regulates lipid metabolism and antigen presentation by tDCs
- Silencing XBP1 in tDC extends host survival by enhancing T cell anti-tumor immunity

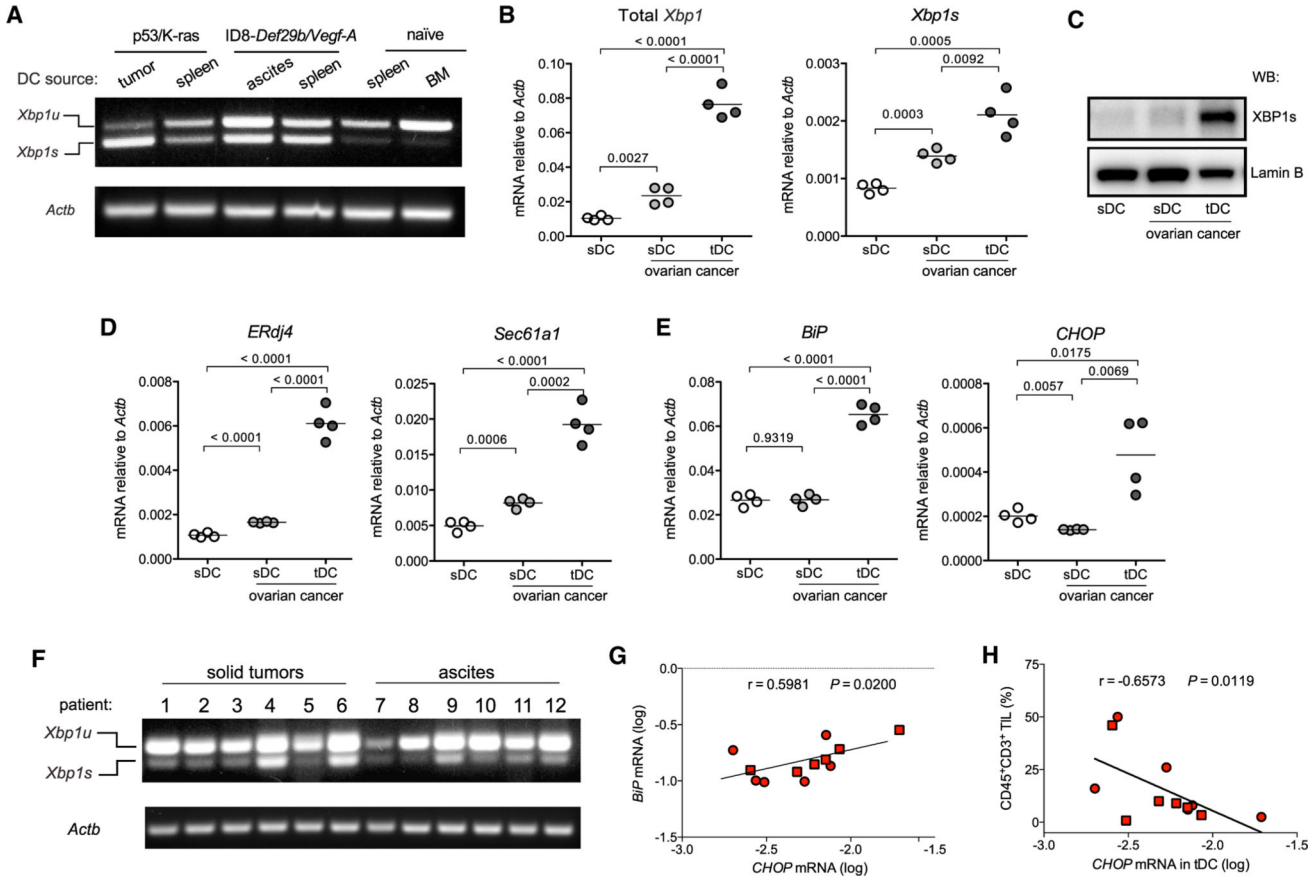

Figure 1. XBP1 Activation in OvCa-Associated DCs

(A) Murine $CD45^+CD11c^+MHC\text{-}II^+CD11b^+CD8\alpha^{low}$ tDCs were isolated from advanced p53/K-ras-driven ovarian tumors or from malignant ascites of mice bearing aggressive ID8-*Defb29/Vegf-A* ovarian carcinoma for 4–5 weeks, and their identity as bona fide classical DCs was confirmed by quantifying *Clec9A/DNGR-1* and *Zbtb46* expression (see also Figure S1). $CD45^+CD11c^+MHC\text{-}II^+CD11b^+CD8\alpha^-$ splenic DCs (sDCs) were isolated from naive or tumor-bearing mice. *Xbp1* splicing was evaluated using conventional RT-PCR. *Xbp1u*, unspliced form; *Xbp1s*, spliced form. (B–E) DCs were isolated from naive mice or from hosts bearing ID8-*Defb29/Vegf-A* OvCa for 3–4 weeks. (B, D, and E) Expression of the indicated transcripts was determined by RT-qPCR, and data were normalized to endogenous levels of *Actb*. (C) Western blot analysis of XBP1s expression in nuclear extracts obtained from the indicated DCs. Lamin B was used as loading control. (F) $CD45^+CD3^-$ $CD20^-$ $CD11c^+DEC205^+$ tDCs were isolated from human patient ovarian tumors or metastatic OvCa ascites samples, and *Xbp1* splicing was evaluated. (G) Expression of *BiP* and *CHOP* by all human tDC samples was analyzed. (H) The proportion of $CD45^+CD3^+$ tumor-infiltrating lymphocytes (TILs) was correlated with tDC *CHOP* mRNA expression in the same human specimen. r, Spearman's rank correlation coefficient.

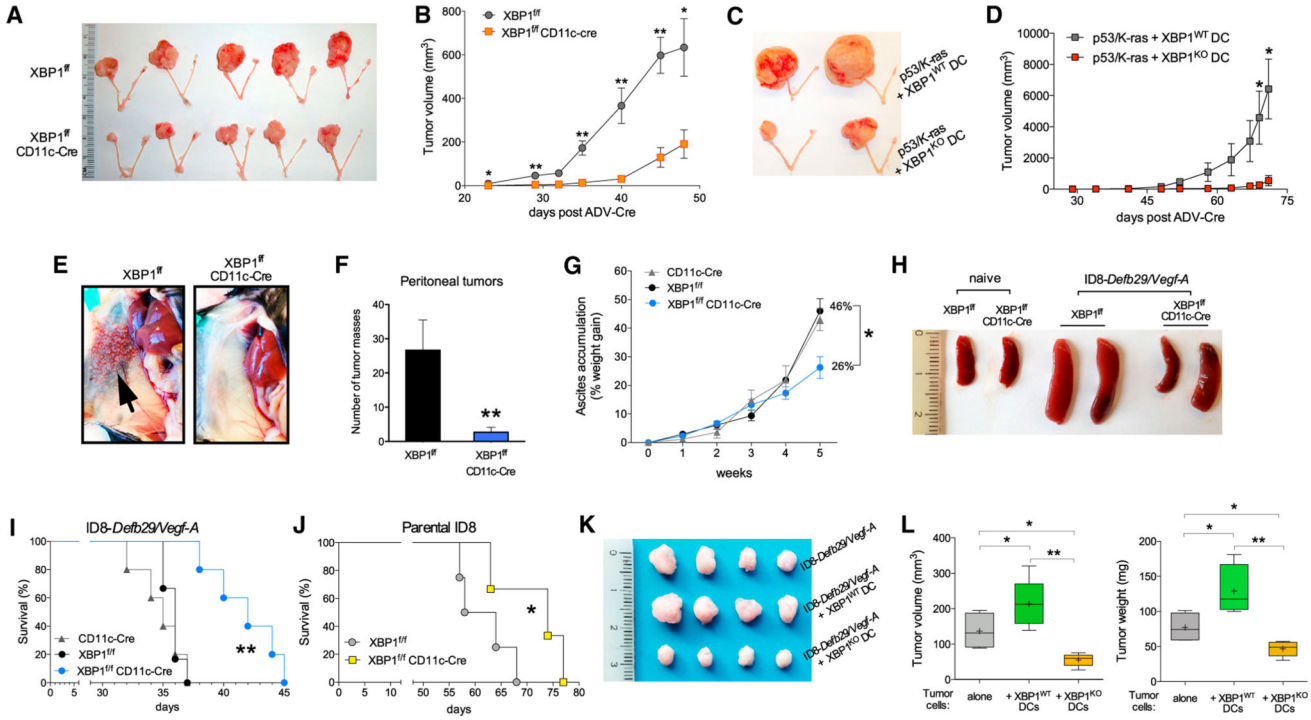

Figure 2. OvCa Progression in Hosts Lacking XBP1 in DCs

(A) p53/K-ras-driven ovarian tumors were generated in hosts reconstituted with BM from either XBP1$^{f/f}$ (top) or XBP1$^{f/f}$ CD11c-Cre (bottom) donor mice. *p53* deletion and oncogenic KRAS expression were induced via intrabursal injection of Cre-expressing adenovirus (ADV-Cre), as described in the Supplemental Experimental Procedures, and primary tumors were resected 7 weeks later. (B) Growth kinetics of p53/K-ras-driven tumors shown in (A). (C and D) Mice bearing primordial p53/K-ras-driven tumors for 28 days were injected i.p. with WT or XBP1-deficient (KO) BMDCs, and tumor growth was monitored over time until day 71. (E–H) Mice of the indicated genotypes were implanted with ID8-*Defb29-VegfA* OvCa cells via i.p. injection. (E and F) Peritoneal metastases evaluated 3–4 weeks after tumor implantation (n = 3 per group). (G) Malignant ascites generation in tumor-bearing mice expressed as percent weight gain due to progressive accumulation of peritoneal fluid. (H) Reduced splenomegaly in tumor-bearing mice deficient for XBP1 in CD11c^{+} DCs. (I and J) Survival in mice bearing aggressive ID8-*Defb29-VegfA* (I) or parental ID8 (J) tumors. Data are representative of at least two independent experiments with similar results using four to six mice per group. (K and L) ID8-*Defb29-VegfA* cancer cells were implanted in the flank alone or in combination with WT or XBP1-deficient (KO) BMDCs. Tumors were resected and measured 40 days later. *p < 0.05, **p < 0.001. Error bars represent SEM.

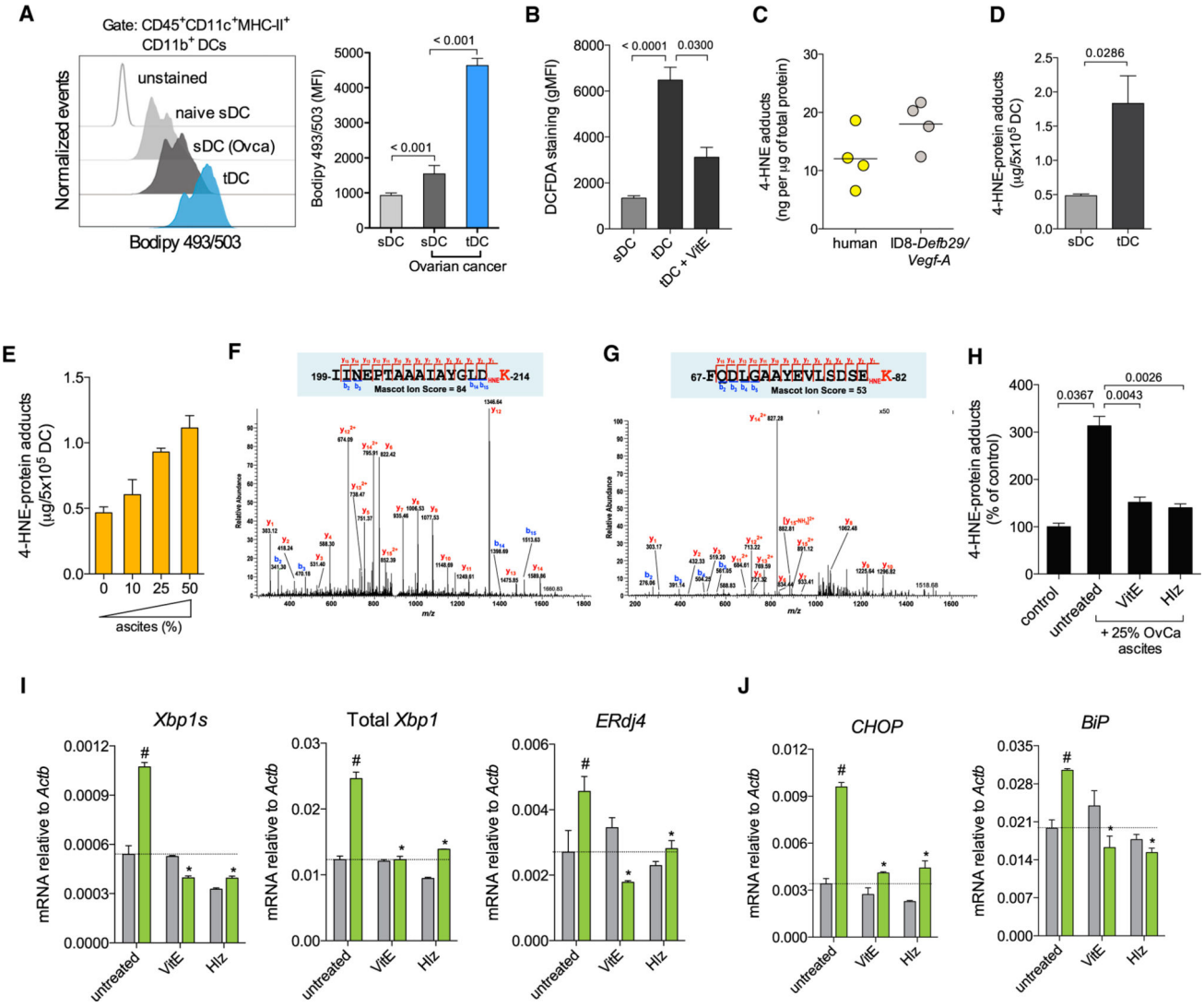

Figure 3. Lipid Peroxidation Byproducts Trigger ER Stress in DCs

(A) Intracellular lipid content in DC populations from naive or tumor-bearing mice (OvCa). (Left) Representative FACS analysis of lipid staining for DCs from the indicated sources. (Right) Lipid quantification expressed as mean fluorescence intensity (MFI) of Bodipy 493/503 staining. (B) Intracellular ROS levels in sDCs or in tDCs untreated or treated with vitamin E (VitE). Data are expressed as geometric MFI (gMFI) of DCFDA staining. (C) Intracellular 4-HNE-protein adducts in tDCs from human or mouse metastatic OvCa ascites samples. (D) Levels of 4-HNE-protein adducts in tDCs compared with control sDCs from tumor-bearing mice. (E) Dose-dependent increase in intracellular 4-HNE-protein adducts in sDCs exposed to ascites supernatants. (F) MS/MS spectrum on the doubly charged precursor at *m/z* 909.00, identifying a tryptic peptide with 4-HNE forming a Michael adduct on the Lys214 residue of the peptide from the 78 kDa glucose-regulated protein precursor (GRP78/ BiP). (G) MS/MS spectrum on the triply charged precursor at *m/z* 643.32, identifying a tryptic peptide with 4-HNE forming a Michael adduct on the Lys82 residue of the peptide from the dnaJ homolog subfamily B member 11 precursor (ERdj3/Dnajb11). (H)

Intracellular levels of 4-HNE protein adducts in sDCs exposed to cell-free ascites in the presence or absence of VitE or Hydralazine (Hlz) for 18 hr. (I and J) tDC were pretreated with VitE or Hlz and then incubated in normal media (gray bars) or in media supplemented with 25% cell-free ascites (green bars) for 18 hr. Expression of the indicated transcripts was assessed via RT-qPCR. Data are normalized to *Actb* expression in each sample. $^{\#}p < 0.05$ compared with tDC in ascites-free media. $*p < 0.05$ compared with ascites-exposed untreated tDC. Error bars represent SEM.

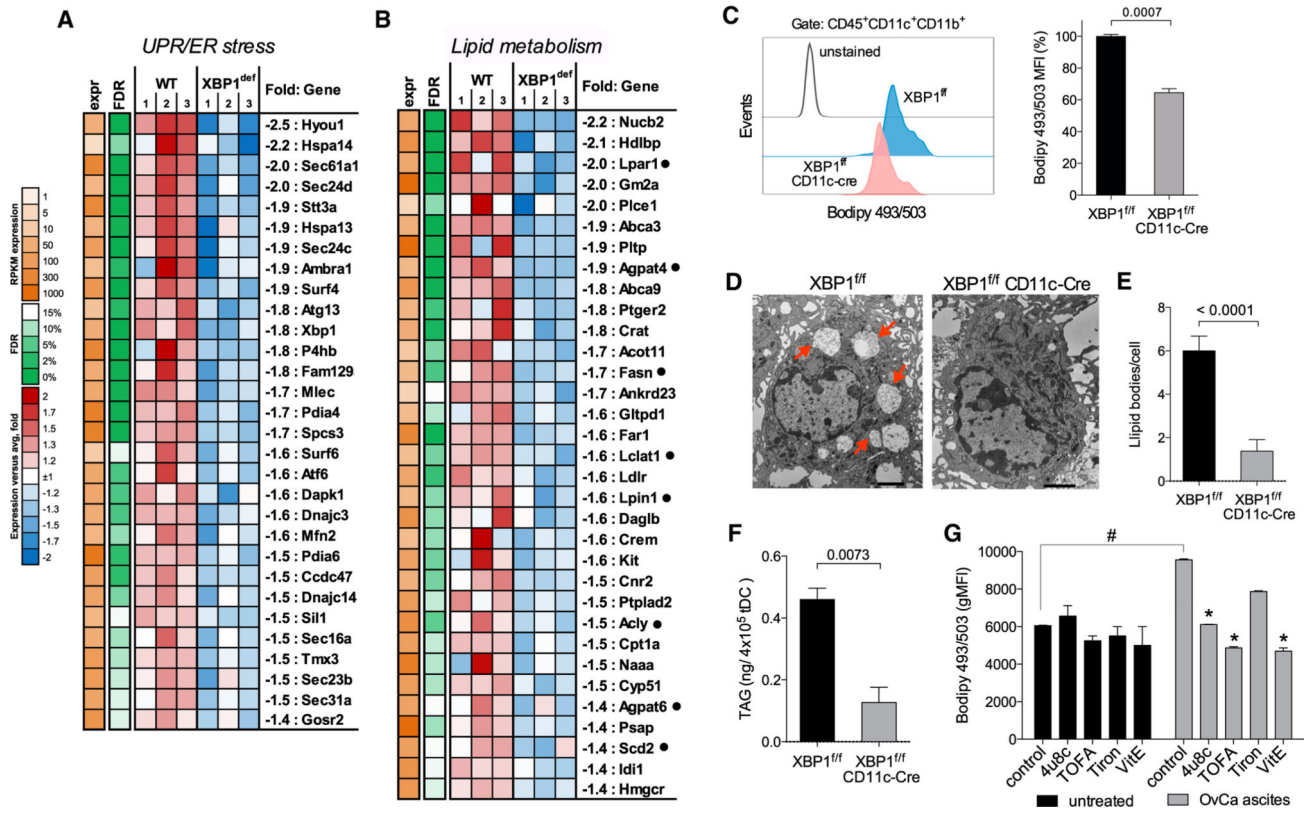

Figure 4. XBP1 Disrupts Lipid Homeostasis in OvCa-Associated DCs

(A and B) Downregulation of genes involved in the UPR/ER stress response (A) and lipid metabolism (B) in tDCs devoid of XBP1. WT is $XBP1^{f/f}$ tDC. $XBP1^{def}$ is $XBP1^{f/f}$ CD11c-Cre tDC (n = 3 per group). Black dots indicate genes involved in triglyceride biosynthesis. (C) Decreased intracellular lipid content in $XBP1^{f/f}$ CD11c-Cre tDCs (n = 3 mice per group) from mice bearing ID8-*Defb29-VegfA* tumors for 3 weeks revealed by Bodipy493/503 staining. (D) Electron micrographs (12,0003) showing large intracellular lipid bodies (red arrows) in XBP1-sufficient, but not XBP1-deficient, tDC. Black scale bars represent 2 μm. (E and F) Quantification of lipid bodies (E) and intracellular triacylglycerides (TAGs) (F) in tDCs sorted from mice bearing ID8-*Defb29-VegfA* ovarian tumors for 3–4 weeks. (G) tDCs were incubated in vitro with or without 25% cell-free OvCa ascites in the presence of 4μ8c, TOFA, Tiron, or VitE. Intracellular lipid content was assessed 24 hr later via Bodipy493/503 staining. Data are representative of three independent experiments with similar results. $^{\#}p < 0.05$ compared with control tDC incubated in the absence of cell-free ascites supernatants. *$p < 0.05$ compared with ascites-exposed tDC but left untreated. Error bars represent SEM.

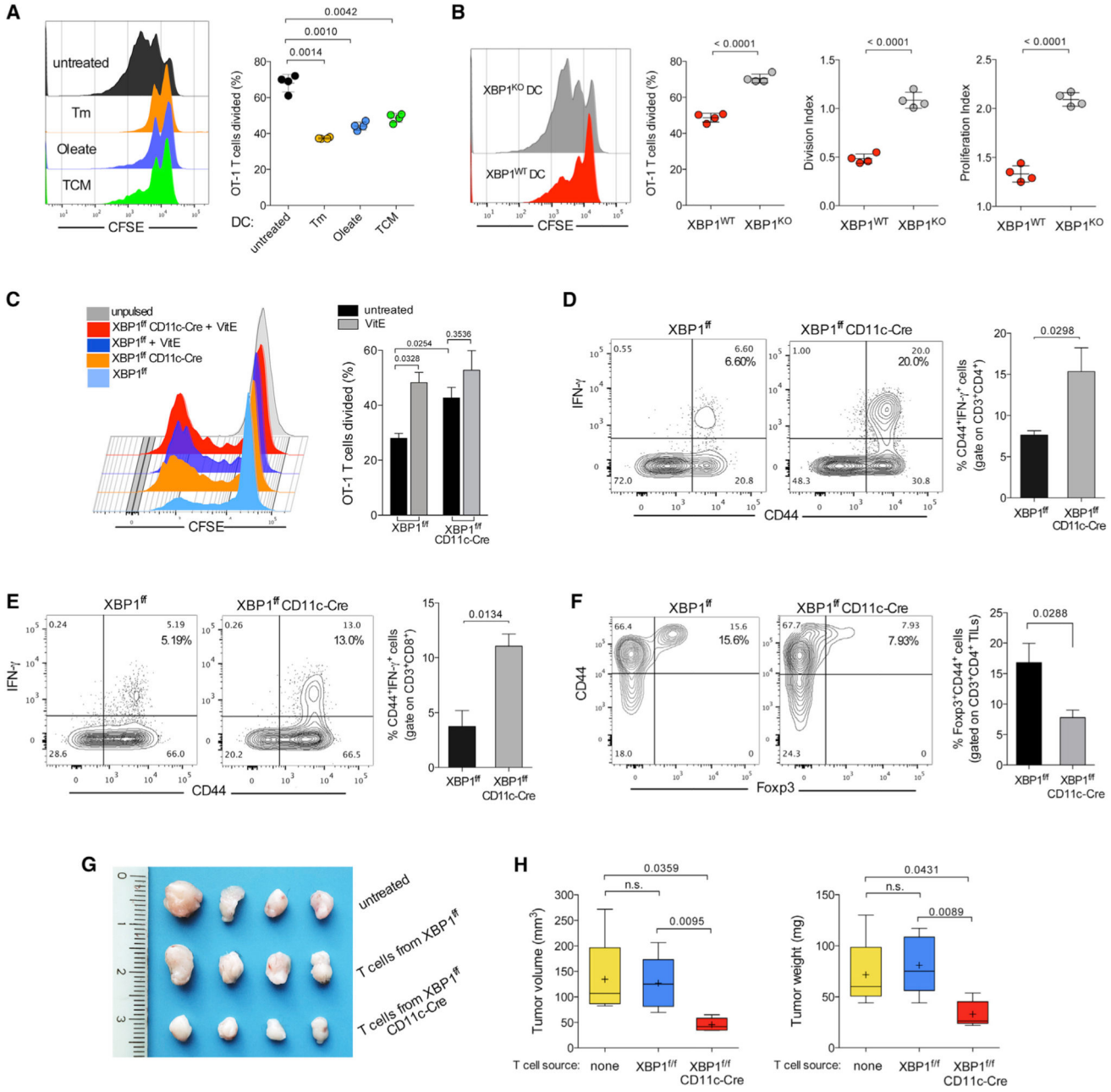

Figure 5. XBP1 Promotes DC Malfunction in the OvCa Microenvironment

(A) WT BMDCs were left untreated or treated with tunicamycin (Tm), oleate, or TCM for 8 hr and then pulsed overnight with 100-μg/ml full-length OVA protein. CFSE-labeled OT-1 T cells were co-cultured with treated BMDCs, and proliferation was assessed by FACS 3 days later. (B) WT or XBP1-deficient (KO) BMDCs were incubated in 25% TCM for 8 hr, and the proliferation assay was repeated as described in (A). (C) CFSE-dilution analysis of OT-1 T cells co-cultured with OVA protein-pulsed tDCs isolated from the peritoneal cavity of $XBP1^{f/f}$ or $XBP1^{f/f}$ CD11c-Cre mice bearing ID8-*Defb29*-*VegfA* ovarian tumors for 4 weeks. tDCs were treated or untreated with vitamin E (VitE) during the OVA pulse. (D and E) Enhanced endogenous T cell activation at tumor sites in mice devoid of XBP1 in tDCs.

Peritoneal wash samples from WT (XBP1$^{f/f}$, black bars) or XBP1-deficient (XBP1$^{f/f}$ CD11c-Cre, gray bars) mice were collected 2–3 weeks after peritoneal implantation of ID8-*Defb29-VegfA* OvCa cells. Surface expression of CD44 and intracellular levels of tumoricidal IFN-γ were analyzed on $CD3^+CD4^+$ (D) or $CD3^+CD8^+$ (E) tumor-infiltrating T cells (TILs). (F) Proportion of T regulatory cells at tumor locations in mice of the indicated genotypes bearing metastatic ID8-*Defb29-VegfA* ovarian tumors for 3 weeks. In all cases, data are representative of two independent experiments using three to four mice per group. (G and H) Growth of solid ID8-*Defb29-VegfA* ovarian tumors in hosts adoptively transferred with splenic and draining lymph node T cells isolated from XBP1 $^{f/f}$ or XBP1$^{f/f}$ CD11c-Cre mice bearing metastatic tumors for 30 days. Error bars represent SEM.

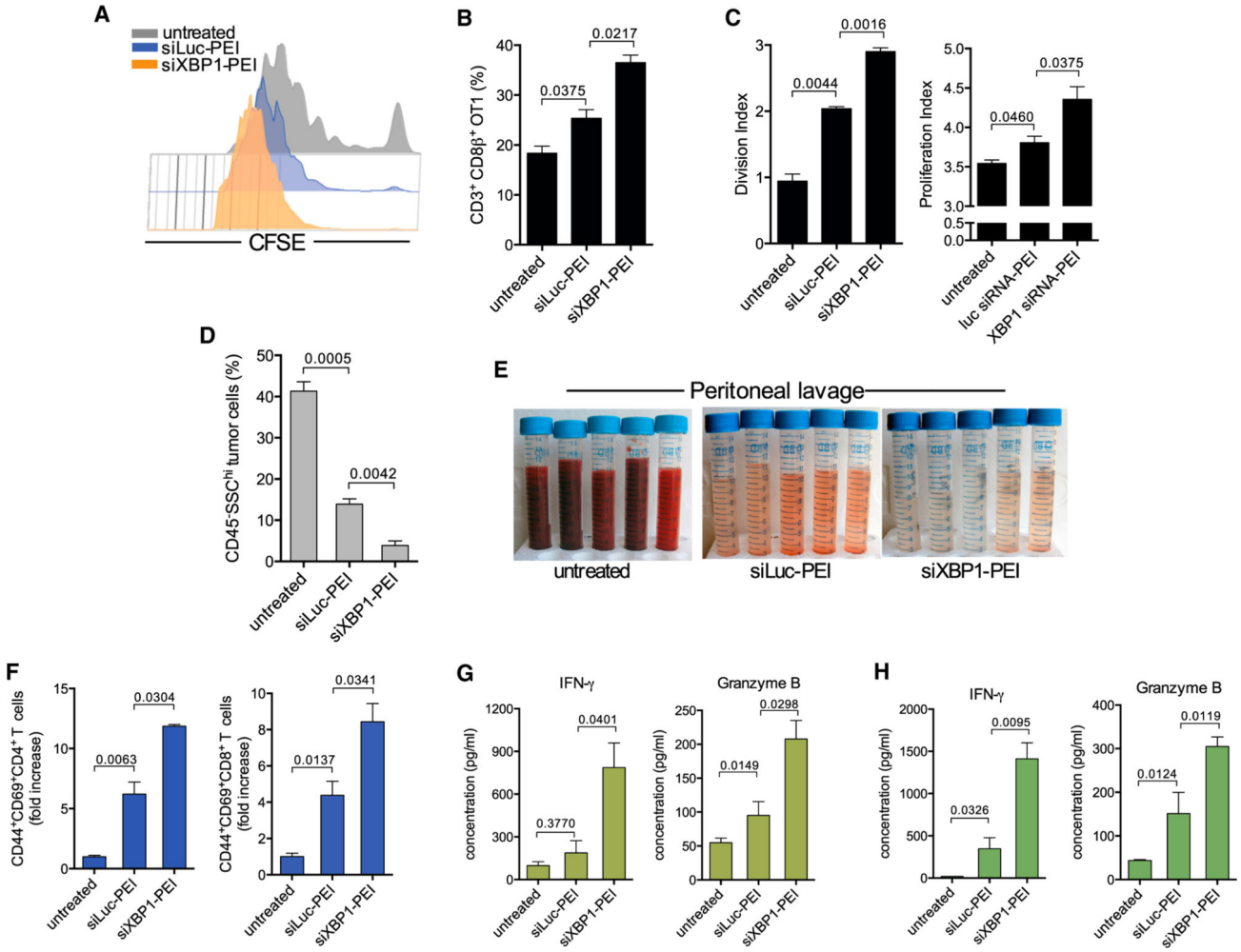

Figure 6. Therapeutic Silencing of XBP1 Improves tDC Function and Evokes Anti-tumor Immunity

(A) Representative CFSE dilution of OT-1 T cells proliferating in vivo at tumor sites in OVA protein-pulsed untreated mice or after administration of immunostimulatory nanocomplexes carrying luciferase-matching (siLuc-PEI) or XBP1-specific (siXBP1-PEI) siRNA. (B) Proportion of OT-1 T cells in ascites of treated mice (n = 3 per group) 3 days after transfer. (C) Division and proliferation index of transferred OT-1 T cells shown in (B). (D–H) Enhanced anti-tumor immune responses in mice treated with DC-targeting, XBP1-silencing nanocomplexes. ID8-*Defb29/Vegf-A* tumor-bearing mice (n = 3 per group) were treated at days 8, 13, 18, and 23 post-tumor injection, and peritoneal lavage samples were analyzed at day 27. (D) Proportion of metastatic tumor cells ($CD45^{-}$ SSC^{hi}) found in the peritoneal cavity of treated mice. (E) Representative pictures of peritoneal lavages obtained from treated mice. (F) Proportion of antigen-experienced ($CD44^{+}$), activated ($CD69^{+}$) $CD4^{+}$ (left), and $CD8^{+}$ (right) T cells infiltrating tumor locations determined by FACS analyses (gated on $CD3^{+}$ cells). (G and H) Representative ELISA-based analysis showing increased IFN-γ and Granzyme B secretion by peritoneal (G) and splenic (H) T cells isolated from mice treated with XBP1-silencing nanoparticles. Error bars represent SEM.

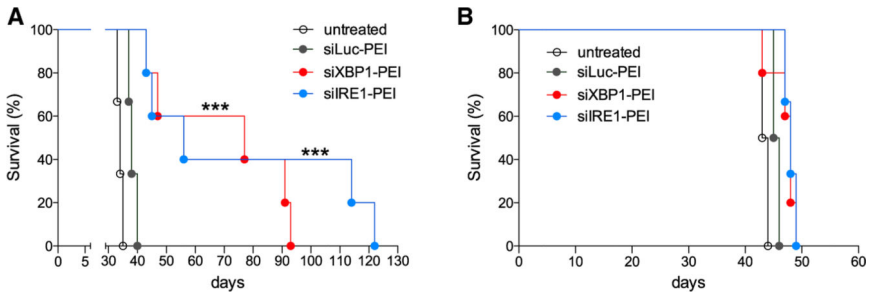

Figure 7. Therapeutic Effects of Targeting IRE1α/XBP1 Signaling in OvCa DCs

(A and B) Survival analysis in WT (A) or *Rag2*-deficient (B) OvCa-bearing mice (n = 6 per group) treated with nanocomplexes at days 12, 16, 20, 24, 28, and 32 after implantation of ID8-*Defb29/Vegf-A* cancer cells. Data are representative of two independent experiments with similar results. ***p < 0.001, log-rank test.